# Positioning and Data Broadcasting using Illumination Pattern Sequences Displayed by LED Arrays

Johannes Herrnsdorf, *Member, IEEE*, Martin D. Dawson, *Fellow, IEEE*, and Michael J. Strain, *Member, IEEE*

**Abstract**

Illumination of a scene with a time-sequence of spatial light patterns enables clients within the scene to navigate, receive broadcast wireless data, or make subsequent space-division multiple access connections to a high bandwidth wireless system. We have developed dedicated binary pattern sequences, for use with arrays of light-emitting diodes (LEDs), which are projected on the area of interest. The LED arrays can be in either active-matrix or matrix-addressable format. The properties of the different sequences are compared theoretically and experimentally, highlighting a trade-off between position update rate and resilience against pixel cross-talk and interference.

**Index Terms**

light-emitting diodes (LEDs), localization, wireless optical, position measurement, navigation.

J. Herrnsdorf, M. Strain and M. Dawson are with the Institute of Photonics, Department of Physics, University of Strathclyde, Glasgow G1 1RD, UK (e-mail: johannes.herrnsdorf@strath.ac.uk).

The authors thank the Engineering and Physical Sciences Research Council for funding under the grant EP/M01326X/1, QuantIC. The underlying data for this work can be found at [1].

Manuscript received April 19, 2005; revised August 26, 2015.

# I. INTRODUCTION

Navigation in areas outside global positioning system coverage is a topic of great interest for both human users and also for the control of automated systems and robots. For example, indoors or underwater environments do not yet have established navigation methods that provide similar accuracy and convenience as the global positioning system. Therefore, instead of relying on global positioning, such environments will benefit from the development of local navigation aids. Such local systems could potentially be scaled to fit particular applications, from meter-scale precision down to microscopic ranges. A promising approach for a local wireless positioning system is the employment of visible light communications (VLC) where the navigation area is illuminated with light-emitting diodes (LEDs) that are intensity-modulated to provide a wireless-optical data signal [2], [3].

Various methods of using VLC for positioning have been demonstrated, including triangulation, time difference of arrival, optical fingerprint signals, and probabilistic methods [2]. Each of these approaches have specific benefits and limitations. Here, we focus on fingerprint signals that are supplied by an array of LEDs [4]–[6] as shown schematically in Fig. 1. The array output is projected onto the area of interest and illuminates it with a time-sequence of spatial illumination patterns, providing convenient scalability of the projection area to adapt to different applications. Flicker-free illumination is enabled by pattern update rates of up to 30 kfps [7]. If the illumination pattern sequence is chosen appropriately, then it provides a unique optical fingerprint signal for each location in the area and thus enables the determination of position. The basic principle of such positioning has been demonstrated experimentally with an active-matrix LED array where the optical fingerprint was a simple Manchester-encoded bit sequence [4]. Notably, a great range of possible pattern sequences can in principle be employed for positioning, including raster-scanning and the Hadamard basis [8]. Therefore, dedicated engineering of the pattern sequences is crucial to optimize the system performance.

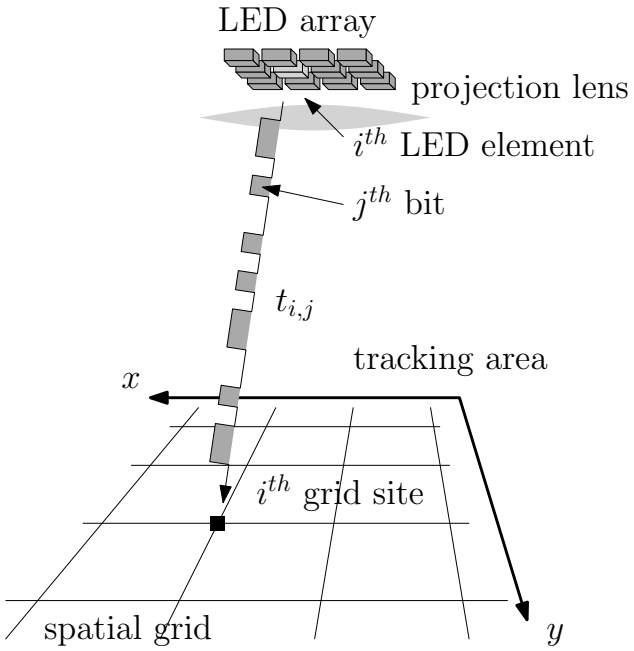


Fig. 1. Schematic of positioning via fingerprint optical signals from an LED array. The $i^{th}$ LED element is projected to the $i^{th}$ site of the spatial grid in the $x-y$ plane, and it is modulated with a fingerprint bit sequence $t_{i,j}$.

Here, we develop construction methods for a number of dedicated pattern sequences for positioning with LED arrays. The construction method in section III-A is independent of the array geometry and in sections III-B and IV-A further methods for rectangular arrays are discussed. All the generated pattern sequences enable positioning with minimal requirement of processing resources at the receiver end and also offer potential dual use for lighting and compatibility with dimming is demonstrated. We investigate short sequences for high position upate rates and longer sequences that provide increased resilience against optical cross-talk and interference. The susceptibility of the pattern sequences to cross-talk and interference is assessed using a theoretical figure of merit as well as direct experimental comparison. A scheme to enable the broadcasting of data interleaved with the positioning signal is also presented. Notably, all desired properties can be met with pattern sequences that are compatible with passive-matrix addressable LED arrays [9], [10] taking advantage of simpler fabrication and higher technology maturity

compared to active-matrix devices. Although not being a specific design target, the sequences use Manchester encoding which is well-aligned with current trends for low bitrate VLC systems [11], [12].

## II. General considerations

We consider an illumination system following the schematic of Fig. 1 where $N$ modulated illumination elements are imaged onto the illumination area such that each element illuminates exactly one site of a spatial grid. Each element is modulated with a unique bit sequence of length $n$ and any device within the illuminated area can locate its position within the grid by measuring the incident light and identifying the bit sequence it is illuminated with. Here we consider that the bits are transmitted using on-off keying because other modulation formats are currently difficult to use with a large array of transmitting LEDs.

Several properties of the illumination sequence are desired. Each element (denoted by index $i$) displays a bit sequence $t_{i,j}$ (where the index $j$ is the bit number):

$$t_{i,j} \in \{0,1\}, \quad i = 1,\ldots,N \quad j = 1,\ldots,n \tag{1}$$

This bit sequence is unique for each element, *i.e.* it provides a unique fingerprint signal at each spatial grid location:

$$\forall i_1 \neq i_2 \exists j : t_{i_1,j} \neq t_{i_2,j} \tag{2}$$

For uniform illumination we require that each element has the same duty cycle of $T_{seq}/n$:

$$\sum_{j=1}^{n} t_{i,j} \equiv T_{seq}, \forall i \tag{3}$$

To minimise effects of electrical cross-talk [13] it is ideal if at each point in time the exact same number $T_{pat}$ of elements is switched on:

$$\sum_{i=1}^{N} t_{i,j} \equiv T_{pat}, \forall j \tag{4}$$

Equation (4) is less important than equations (2) and (3) because the issue it addresses can also be mitigated by hardware engineering. Notably though, the pattern sequences developed here fulfil equation (4) and we did not identify any drawback imposed by this.

For simplicity, we consider that the number $N$ of emitters is a power of 2:

$$N = 2^m \tag{5}$$

This is a natural choice due to the binary encoding of the position information. Generalization to other numbers of $N$ is achieved by choosing the next higher power of 2:

$$m_{equiv} = \lceil \log_2(N) \rceil$$

and then using an adequate subset of the bit sequences which are described in the following sections.

### A. General Properties

From the basic requirements (2), (3) and (4) there follow some properties of the pattern sequences that are not obvious. Proofs of these properties are provided in the appendix.

The duty cycle of each pixel and the number of pixels switched on in each pattern are linked to each other:

$$T_{seq} = \frac{n}{2^m} T_{pat} \tag{6}$$

The length of the pattern sequence is an even number:

$$n \text{ is even}, \quad n = 2k, \quad k \in \mathbb{N} \tag{7}$$

The shortest possible sequence length $n_{min}$ fulfilling equations (2) and (3) is given by:

$$n_{min} = \min \left( \left\{ n \in \mathbb{N}, \binom{n}{\lfloor n/2 \rfloor} \geq 2^m \right\} \right) \tag{8}$$

For infinitely many emitters this approaches $m + 1$:

$$\lim_{N \to \infty} n_{min} = m + 1 \tag{9}$$

However, this limit is approached very slowly and for all practical numbers of emitters the minimum length is close to $2m$:

$$n_{min}|_{practical} \approx 2m \tag{10}$$

## III. Sequences of minimal length

Equations (9) and (10) indicate that pattern sequences that scale logarithmically with the number of emitters provide, in good approximation, the shortest possible sequence lengths. In this section, we present two approaches to generate pattern sequences of length $2m$ and $3m$.

### A. Patterns generated by induction

A pattern sequence with a length of $n = 2m$ can be created by an induction method. For $m = 1$, there are two locations and two unique bit sequences of length $n = 2$ which fulfil all requirements:

$$t^{(1)} = \begin{bmatrix} 1 & 0 \\ 0 & 1 \end{bmatrix} \tag{11}$$

Where $t^{(1)}$ is the matrix of bit sequences for $m = 1$.

Induction step: For a given $m$ the matrix $t^{(m)}$ of bit sequences is known:

$$t^{(m)} = \begin{bmatrix} t^{(m)}_{1,1} & t^{(m)}_{1,2} & \dots & t^{(m)}_{1,2m} \\ t^{(m)}_{2,1} & t^{(m)}_{2,2} & \dots & t^{(m)}_{2,2m} \\ \vdots & & & \\ t^{(m)}_{2^m,1} & t^{(m)}_{2^m,2} & \dots & t^{(m)}_{2^m,2m} \end{bmatrix} \tag{12}$$

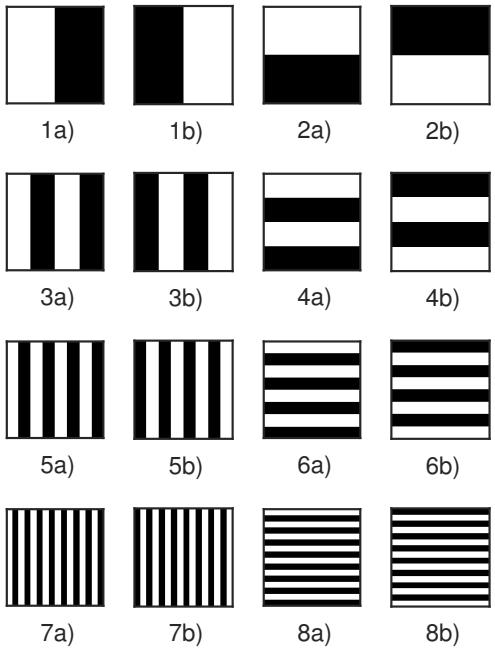


Fig. 2. Pattern sequence A. 16×16 pattern sequence created by the approach described in section III-A. Note that this is also equivalent to the binary search pattern when using $B^{(1)}, B^{(2)}$ of equation (14). The patterns are numbered in pairs, where a) and b) refer to two patterns that are the inverse of each other.

Then for $m \to m+1$, the following matrix $t^{(m+1)}$ fulfils all conditions (2), (3) and (4):

$$t^{(m+1)} = \begin{bmatrix} t_{1,1}^{(m)} & t_{1,2}^{(m)} & \dots & t_{1,2m}^{(m)} & 1 & 0 \\ t_{1,1}^{(m)} & t_{1,2}^{(m)} & \dots & t_{1,2m}^{(m)} & 0 & 1 \\ t_{2,1}^{(m)} & t_{2,2}^{(m)} & \dots & t_{2,2m}^{(m)} & 1 & 0 \\ t_{2,1}^{(m)} & t_{2,2}^{(m)} & \dots & t_{2,2m}^{(m)} & 0 & 1 \\ \vdots & & & & & \\ t_{2^m,1}^{(m)} & t_{2^m,2}^{(m)} & \dots & t_{2^m,2m}^{(m)} & 1 & 0 \\ t_{2^m,1}^{(m)} & t_{2^m,2}^{(m)} & \dots & t_{2^m,2m}^{(m)} & 0 & 1 \end{bmatrix} \tag{13}$$

Note that these sequences have a length of $n^{(m+1)} = 2(m+1)$.

An example of a sequence for a representative 16×16 emitter array created by this approach

is shown in Fig. 2 and is referred to as sequence A. In this case, stripe patterns of different spatial frequency are generated. Note that for each pattern, its inverse is also contained in the sequence. Therefore, even though not specified as a design target in section II, it is possible to operate the receiver such that it receives the positioning signal as Manchester encoded bits. Pattern sequence A is the one used in our earlier report on an LED-based positioning system [4] and it is described there how the Manchester encoded bits provide a unique spatial fingerprint.

### *B. Binary search patterns*

Pattern sequence A unintentionally has a remarkable property: it allows the decoding algorithm to be implemented in a binary search fashion. The first four patterns of sequence A allow allocation of the position to one quadrant of the entire array. The next four patterns then allow allocation to one quadrant within the first quadrant and so on until the last four patterns allow positioning with full precision. Here, we describe a more general way of constructing pattern sequences that allow such binary search positioning for square arrays of dimension $2^l \times 2^l$.

Consider the following $2\times2$ matrices:

$$B^{(1)} = \begin{bmatrix} 1 & 0 \\ 1 & 0 \end{bmatrix} \quad B^{(2)} = \begin{bmatrix} 1 & 1 \\ 0 & 0 \end{bmatrix} \quad B^{(3)} = \begin{bmatrix} 1 & 0 \\ 0 & 1 \end{bmatrix} \tag{14}$$

Note that these three patterns correspond to the $2\times2$ Hadamard basis and can therefore be used for $2\times2$ location. In fact, only using $B^{(1)}$ and $B^{(2)}$ is already sufficient for positioning and including $B^{(3)}$ is optional. This $2\times2$ sequence fulfils conditions (2) and (4), but not (3). Therefore, the inverse of each pattern needs to be included.

Pattern sequence A is obtained if the two patterns $B^{(1)}$ and $B^{(2)}$ and their inverses are applied first over the entire area, then within each quadrant and so on until a precision of a single pixel is reached. If additionally pattern $B^{(3)}$ and its inverse are included in the process, the sequence shown in Fig. 3 is obtained which has a slightly longer length of $n = 3m$ and is referred to

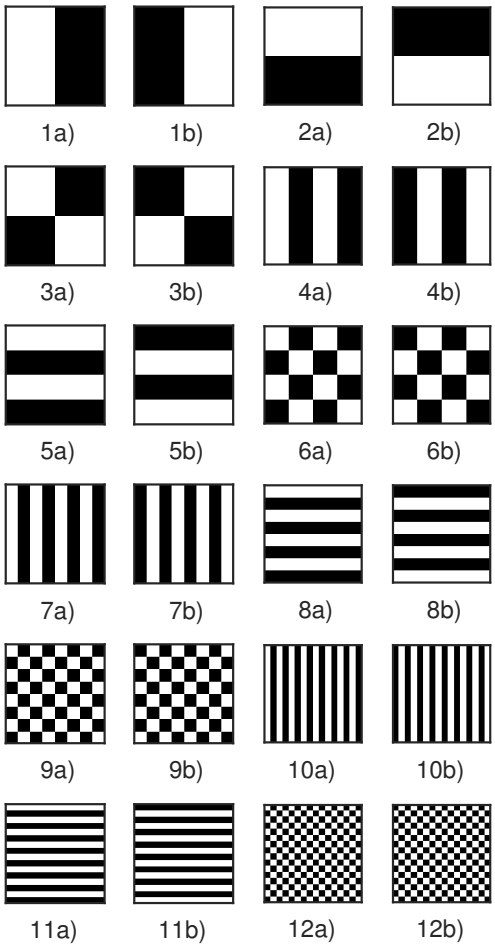


Fig. 3. Pattern sequence B. 16×16 binary search patterns using $B^{(1)}, B^{(2)}, B^{(3)}$ of equation (14). The patterns are numbered in pairs, where a) and b) refer to two patterns that are the inverse of each other.

as sequence B. The detailed procedure to construct these sequences from $B^{(1)}$, $B^{(2)}$ and $B^{(3)}$ is given in equation (15).

$$t_{\cdot,i} = \begin{bmatrix} B_{1,1}^{(i)} & \cdots & B_{1,1}^{(i)} & B_{1,2}^{(i)} & \cdots & B_{1,2}^{(i)} \\ \vdots & & \vdots & \vdots & & \vdots \\ \underbrace{B_{1,1}^{(i)} \quad \cdots \quad B_{1,1}^{(i)}}_{2^{l-1}\times 2^{l-1}} & & & \underbrace{B_{1,2}^{(i)} \quad \cdots \quad B_{1,2}^{(i)}}_{2^{l-1}\times 2^{l-1}} & & \\ B_{2,1}^{(i)} & \cdots & B_{2,1}^{(i)} & B_{2,2}^{(i)} & \cdots & B_{2,2}^{(i)} \\ \vdots & & \vdots & \vdots & & \vdots \\ \underbrace{B_{2,1}^{(i)} \quad \cdots \quad B_{2,1}^{(i)}}_{2^{l-1}\times 2^{l-1}} & & & \underbrace{B_{2,2}^{(i)} \quad \cdots \quad B_{2,2}^{(i)}}_{2^{l-1}\times 2^{l-1}} & & \end{bmatrix}$$

$$t_{\cdot,i+3} = \begin{bmatrix} B_{1,1}^{(i)} & \cdots & B_{1,2}^{(i)} & \cdots & B_{1,1}^{(i)} & \cdots & B_{1,2}^{(i)} & \cdots \\ \underbrace{\vdots}_{2^{l-2}\times 2^{l-2}} & & \underbrace{\vdots}_{2^{l-2}\times 2^{l-2}} & & \underbrace{\vdots}_{2^{l-2}\times 2^{l-2}} & & \underbrace{\vdots}_{2^{l-2}\times 2^{l-2}} & \\ B_{2,1}^{(i)} & \cdots & B_{2,2}^{(i)} & \cdots & B_{2,1}^{(i)} & \cdots & B_{2,2}^{(i)} & \cdots \\ \underbrace{\vdots}_{2^{l-2}\times 2^{l-2}} & & \underbrace{\vdots}_{2^{l-2}\times 2^{l-2}} & & \underbrace{\vdots}_{2^{l-2}\times 2^{l-2}} & & \underbrace{\vdots}_{2^{l-2}\times 2^{l-2}} & \\ B_{1,1}^{(i)} & \cdots & B_{1,2}^{(i)} & \cdots & B_{1,1}^{(i)} & \cdots & B_{1,2}^{(i)} & \cdots \\ \underbrace{\vdots}_{2^{l-2}\times 2^{l-2}} & & \underbrace{\vdots}_{2^{l-2}\times 2^{l-2}} & & \underbrace{\vdots}_{2^{l-2}\times 2^{l-2}} & & \underbrace{\vdots}_{2^{l-2}\times 2^{l-2}} & \\ B_{2,1}^{(i)} & \cdots & B_{2,2}^{(i)} & \cdots & B_{2,1}^{(i)} & \cdots & B_{2,2}^{(i)} & \cdots \\ \underbrace{\vdots}_{2^{l-2}\times 2^{l-2}} & & \underbrace{\vdots}_{2^{l-2}\times 2^{l-2}} & & \underbrace{\vdots}_{2^{l-2}\times 2^{l-2}} & & \underbrace{\vdots}_{2^{l-2}\times 2^{l-2}} & \end{bmatrix}$$

$$\vdots$$

$$t_{\cdot,i+3(l-1)} = \begin{bmatrix} B_{1,1}^{(i)} & B_{1,2}^{(i)} & B_{1,1}^{(i)} & B_{1,2}^{(i)} & \cdots & B_{1,1}^{(i)} & B_{1,2}^{(i)} \\ B_{2,1}^{(i)} & B_{2,2}^{(i)} & B_{2,1}^{(i)} & B_{2,2}^{(i)} & \cdots & B_{2,1}^{(i)} & B_{2,2}^{(i)} \\ B_{1,1}^{(i)} & B_{1,2}^{(i)} & B_{1,1}^{(i)} & B_{1,2}^{(i)} & \cdots & B_{1,1}^{(i)} & B_{1,2}^{(i)} \\ B_{2,1}^{(i)} & B_{2,2}^{(i)} & B_{2,1}^{(i)} & B_{2,2}^{(i)} & \cdots & B_{2,1}^{(i)} & B_{2,2}^{(i)} \\ \vdots & \vdots & \vdots & \vdots & & \vdots & \vdots \\ B_{1,1}^{(i)} & B_{1,2}^{(i)} & B_{1,1}^{(i)} & B_{1,2}^{(i)} & \cdots & B_{1,1}^{(i)} & B_{1,2}^{(i)} \\ B_{2,1}^{(i)} & B_{2,2}^{(i)} & B_{2,1}^{(i)} & B_{2,2}^{(i)} & \cdots & B_{2,1}^{(i)} & B_{2,2}^{(i)} \end{bmatrix}$$

$$i = 1, 2, 3 \tag{15}$$

### C. Reordering

If either the order of the sequence is changed or the assignment of bitstreams to individual emitters is changed, then equations (2), (3) and (4) are still fulfilled. Fig. 4 shows an example (sequence C) of how the assignment of bitstreams to pixels can be changed. In particular, Fig. 4 illustrates a set of quasi-randomised patterns suitable for location. An advantage of these patterns may be reduced flicker when transmitting at low frame rates.

## IV. Resilience against optical cross-talk and interference

Note that sequences A and C provide bitstreams with minimal length. Therefore, a single bit error will inevitably result in a spurious position reading, which can only be mitigated by filtering methods such as median filtering of several position readings. Longer sequences enable advanced methods to mitigate bit errors. For example, the position information in sequence B can be obtained by an inverse Hadamard transform of the received signal [8]. In this section, we develop a pattern sequence that mitigates the most common types of bit errors in our experiments, namely bit errors due to optical cross-talk and channel interference.

Experimentally it is observed that “coarse” patterns, i.e. patterns with low spatial frequencies, yield a better signal to noise ratio (SNR). For example, the first four patterns of sequence A

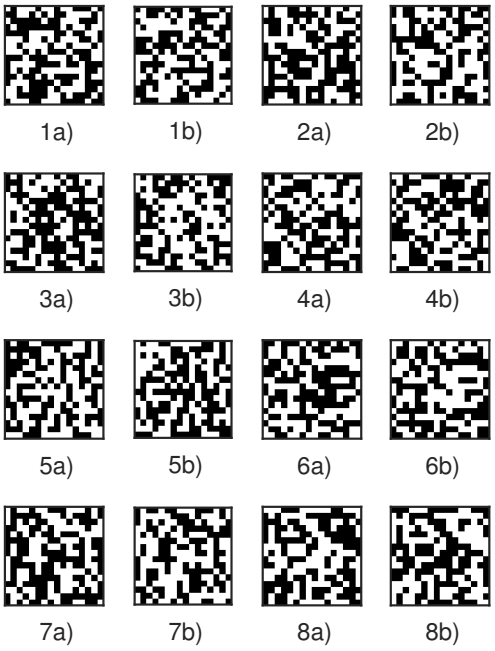


Fig. 4. Pattern sequence C. Equivalent to pattern sequence A but with 500 random pixel pairs swapped as described in section III-C. The patterns are numbered in pairs, where a) and b) refer to two patterns that are the inverse of each other.

experimentally yielded a larger differential signal than the other patterns in this sequence as is shown below in the experimental section V-A (Fig. 7a) and b)). The observed drop in the differential signal can be caused by optical crosstalk between the LED pixels on the chip, and also by interference between the LEDs through overlapping beam profiles. This effect is similar to reported issues with noise in single pixel imaging which are mitigated by dedicated pattern engineering [14], [15]. Therefore, in systems that are affected by optical crosstalk and interference it is a good approach to not use finer and finer meshes but instead use coarse patterns which can be obtained by spatial shifting as described below.

For a given illumination pattern $t_{:,J}$, we can assess its susceptibility to optical crosstalk by a figure of merit $FOM$ as defined in Eq. (16), where a small value of $FOM$ indicates that on

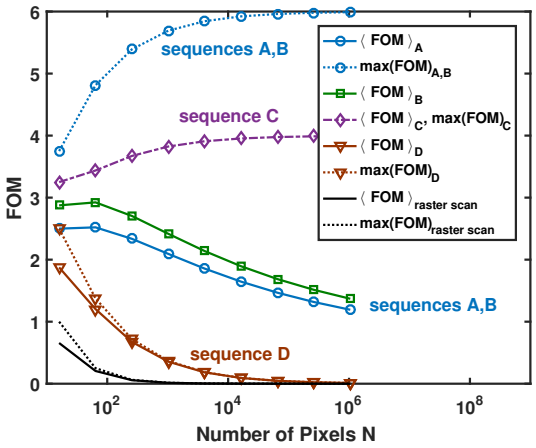


Fig. 5. Figures of merit for resilience against optical crosstalk, $\langle FOM \rangle$ and $\max(FOM)$, for sequences A, B, C, D and raster scanning as a function of pixel number. Note that for sequences of type C, due to their randomized nature, the probabilistic average is plotted, whereas for the other sequences the precise values are known.

the average of all grid sites the pattern has a low risk of bit errors due to optical crosstalk:

$$FOM = \sum_{i=1}^{N} \sum_{j \neq i} w(d(i,j))(1 - \delta_{t_{i,J}, t_{j,J}}) \tag{16}$$

where $d(i,j)$ is a metric for the spatial separation between pixels $i$ and $j$, $w(d(i,j))$ is a weight, and $\delta_{\cdot,\cdot}$ is the Kronecker-$\delta$. The weight function $w(d(i,j))$ should ideally be chosen such that it resembles the spatial dependence of the optical crosstalk. In the case of square arrays, a simple generic choice is:

$$w(d(i,j)) = \begin{cases} 1/N, & \text{pixels } i \text{ and } j \text{ adjacent} \\ 0, & \text{else} \end{cases} \tag{17}$$

In this case, the $FOM$ is the average number of adjacent pixels with different on/off state. For the particular LED arrays used here in the experimental section V-A below, this choice is justified by earlier measurements of the optical cross-talk by Zhang *et al.* [16].

As figures of merit for an entire pattern sequence, we use the average $\langle FOM \rangle$ of all the patterns contained in the sequence and the value of the worst pattern $\max(FOM)$. These two

values can be calculated analytically from Eqs. (16) and (17) and are plotted in Fig. 5. The corresponding analytical expressions are given in the appendix. The scaling behaviors $\langle FOM\rangle_\infty$ and $FOM_\infty$ in the limit of infinitely large $n \times n$ arrays are listed in Tab. I and calculated by Eq. (18):

$$\begin{aligned}\langle FOM\rangle_\infty &= \lim_{n\to\infty} \langle FOM\rangle \\ FOM_\infty &= \lim_{n\to\infty} \max(FOM)\end{aligned} \tag{18}$$

Note that sequences A and B do not differ significantly in $FOM$ and sequence C has on average even worse $FOM$. Therefore, optimization of this aspect requires development of further pattern sequences.

### A. *Moving bars*

A complete positioning sequence comprising coarse patterns can be achieved by taking the first four patterns of sequence A and shifting them horizontally and laterally through the scene. Such a sequence can be constructed from the matrices $B^{(1)}$ and $B^{(2)}$ in equation (14). In a first instance, they are used ot create the initial two patterns:

$$t^{(i)} = \begin{bmatrix} B^{(i)}_{1,1} & \cdots & B^{(i)}_{1,1} & B^{(i)}_{1,2} & \cdots & B^{(i)}_{1,2} \\ \vdots & & \vdots & \vdots & & \vdots \\ \underbrace{B^{(i)}_{1,1} \quad \cdots \quad B^{(i)}_{1,1}}_{2^{l-1}\times 2^{l-1}} & & & \underbrace{B^{(i)}_{1,2} \quad \cdots \quad B^{(i)}_{1,2}}_{2^{l-1}\times 2^{l-1}} & & \\ B^{(i)}_{2,1} & \cdots & B^{(i)}_{2,1} & B^{(i)}_{2,2} & \cdots & B^{(i)}_{2,2} \\ \vdots & & \vdots & \vdots & & \vdots \\ \underbrace{B^{(i)}_{2,1} \quad \cdots \quad B^{(i)}_{2,1}}_{2^{l-1}\times 2^{l-1}} & & & \underbrace{B^{(i)}_{2,2} \quad \cdots \quad B^{(i)}_{2,2}}_{2^{l-1}\times 2^{l-1}} & & \end{bmatrix}$$

$$i = 1, 2 \tag{19}$$

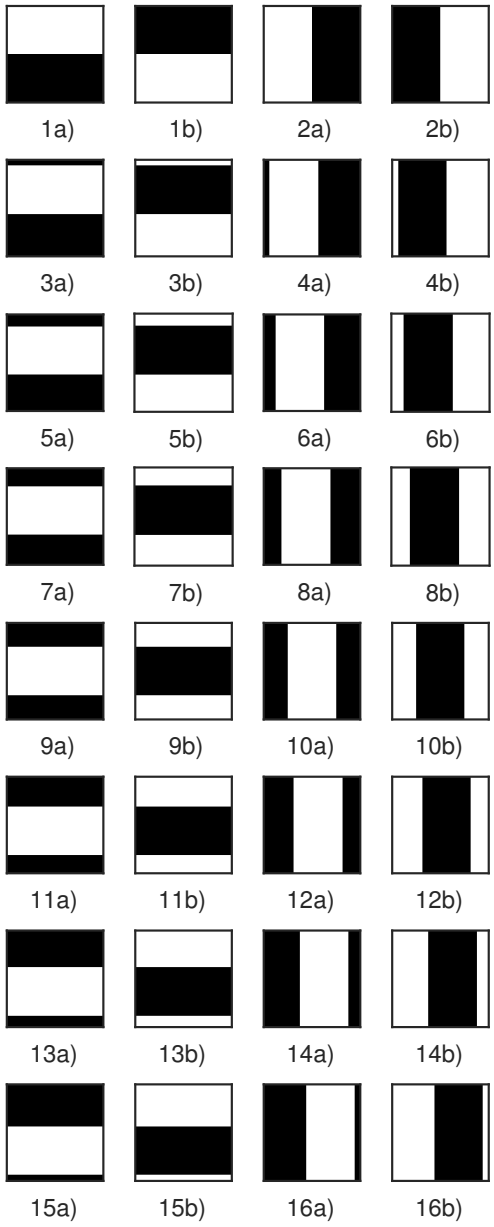


Fig. 6. Pattern sequence D according to equation (20) for a 16×16 array. The patterns are numbered in pairs, where a) and b) refer to two patterns that are the inverse of each other.

Then these patterns are periodically shifted across the array

$$t_{p,q}^{(2j+i)} = t_{(p+j-1)\%16+1,(q+j-1)\%16+1}^{(i)}$$
$$i = 1, 2$$
$$j = 1, \ldots, 2^{m/2-1} - 1 \tag{20}$$

where "$\%$" is the modulo operator. Again, each pattern is supplemented by its inverse to achieve a uniform duty cycle which results in a total sequence length of $n = 2^{m/2+1} = 2\sqrt{N}$. In the case of a 16×16 array this results in the 32 patterns shown in figure 6 (sequence D). The receiver can determine its position by a least-squares optimization of the received bit sequence in relation to a set of expected bit sequences, each of which corresponds to one position.

As can be seen in Fig. 5, the $FOM$ of sequence D is significantly improved compared to sequences A, B and C, but not as low as for raster scanning. This graph, together with table I, shows how sequence D provides a trade-off between the optimization of sequence length on one hand and $FOM$ on the other hand.

## V. Properties

### A. Experimental comparison

We first compare the pattern sequences in a configuration with on-chip optical cross-talk and then discuss a case of stronger interference. Patterns sequences A, B, C, and D were projected by a 16×16 active matrix array of blue-emitting LEDs as described by Herrnsdorf *et al.* [4]. A photodiode with 1 MHz bandwidth was placed within the projection area at row 11, column 8 of the spatial grid. Traces of the optical signal were recorded as shown in Fig. 7. Each pattern was displayed for a duration of 5 ms, which is 10 times longer than the limit of the particular LED array used in this experiment [4] in order to minimize hardware-specific effects in the

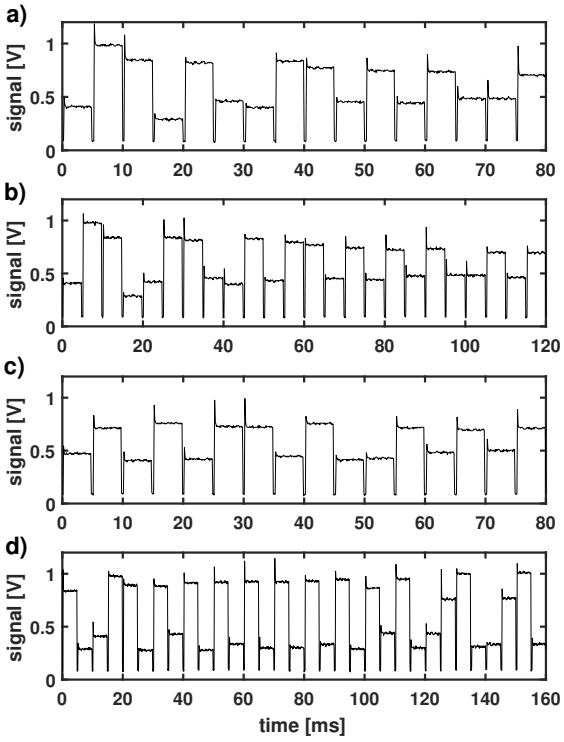


Fig. 7. Representative optical signals received by a photodiode placed at row 11 and column 8 of the 16×16 spatial grid. *a)* Sequence A, *b)* sequence B, *c)* sequence C, and *d)* sequence D.

measurement. 50 samples for each pattern were used to determine the optical powers of the Manchester-encoded information and the noise (which includes receiver noise).

Representative traces are shown in Fig. 7. Figs. 7a) and b) are typical traces when using the binary search type pattern sequences A and B. It can be seen that the first patterns in these two sequences have a stronger intensity contrast between a pattern and its inverse than the last patterns. This is the effect mentioned above in section IV and it is also visible in figure 8a) which plots the differential optical SNR for each pattern pair. The first few patterns of sequences A and B yield an SNR of 19 dB which reduces to 15 dB as the binary search resolution gets finer. This reduction in SNR correlates with the $FOM$ of the patterns as plotted in Fig. 8b). The

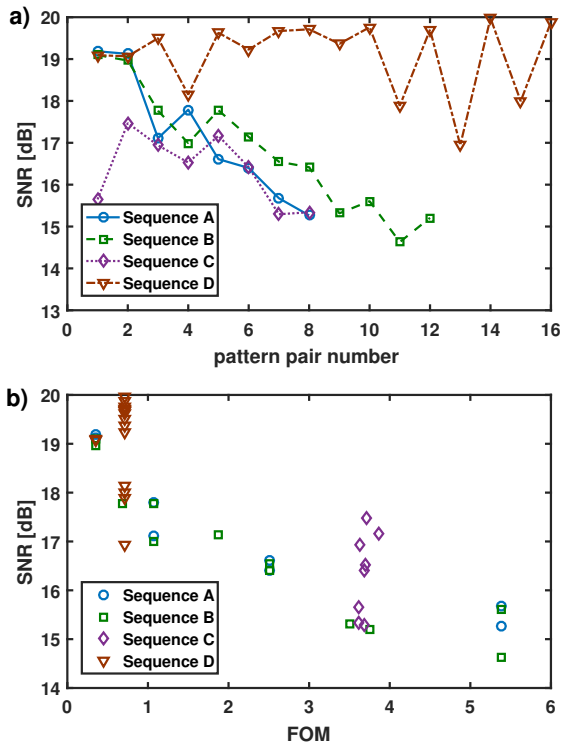


Fig. 8. Experimentally obtained differential SNR of the Manchester-encoded information of each pattern pair measured at position (11,8) of the 16×16 spatial grid, corresponding to the traces shown in figure 7. See also table I. The SNR is plotted as a function of *a)* the pattern labels used in Figs. 2, 3, 4 and 6, and *b)* as a function of the $FOM$ calculated by Eq. (16).

randomized pattern sequence C has less variation in the differential signal of the pattern pairs, see figure 7c). However, the average SNR is comparatively low at 16.4 dB. This aligns well with the observation that the $FOM$ of the patterns is narrowly distributed around the average value of 3.67. Note that the SNR has been measured at only one representative grid position, whereas $FOM$ assesses the average effect on all 256 grid positions. This explains the variation of SNR in sequences C and D despite almost constant $FOM$. The overall trend of decreasing SNR as $FOM$ increases is, however, clearly visible.

When comparing Fig. 7c) to a), b) and d), it can be seen that most of the patterns have a relatively good differential signal. Indeed, in Fig. 8 only 4 of the 16 pattern pairs of sequence D

TABLE I

COMPARISON OF THE DIFFERENT PATTERN SEQUENCES LISTING PATTERN LENGTH, FIGURES OF MERIT FOR THE RESILIENCE AGAINST OPTICAL CROSS-TALK, AND THE EXPERIMENTALLY OBSERVED SNR BASED ON THE DATA SHOWN IN FIGURE 8.

| Sequence | Figure | Number of patterns | $FOM_\infty$ | $\langle FOM\rangle_\infty$ | Maximum SNR | Average SNR | Minimum SNR |
|---|---|---|---|---|---|---|---|
| raster scan | | $N$ | $\frac{16}{N}$ | $\frac{16}{N}$ | | | |
| A | 2 | $2\log_2(N)$ | 6 | $\frac{24}{\log_2(N)}$ | 19.2 dB | 17.4 dB | 15.3 dB |
| B | 3 | $3\log_2(N)$ | 6 | $\frac{248}{9\log_2(N)}$ | 19.1 dB | 17.0 dB | 14.6 dB |
| C | 4 | $2\log_2(N)$ | 4 | 4 | 17.5 dB | 16.4 dB | 15.3 dB |
| D | 6 | $2\sqrt{N}$ | $\frac{12}{\sqrt{N}}$ | $\frac{12}{\sqrt{N}}$ | 20.0 dB | 19.2 dB | 16.9 dB |

have an SNR below 19 dB and the SNR does not drop below 16.9 dB. These 4 pattern pairs are exactly those where the detector position is close to the boundary between regions with LEDs on and off, indicating that indeed cross-talk is responsible for this effect.

Quantitative key figures are listed in table I. Compared to the other sequences, sequence D has an improved SNR by up to 2.8 dB. In particular, the average SNR is improved by around 2 dB and the SNR of the pattern pair with the poorest differential signal is 1.6 dB better compared to all the other sequences.

### *B. Optical Cross-Talk and Interference*

Ideally, the intensity of one LED pixel in the projection area has a constant value within the square given by the projected pixel pitch and is zero elsewhere as indicated by the solid line (i) in Fig. 9a). The real profile was measured with a fibre-coupled spectrometer, where the light was collected by a 1 mm core polymer optical fibre that was moved with a micrometer translation stage across the projected intensity profile. The measured profile (ii) in Fig. 9a) extends clearly into the area of neighbouring pixels, which is primarily due to optical cross-talk

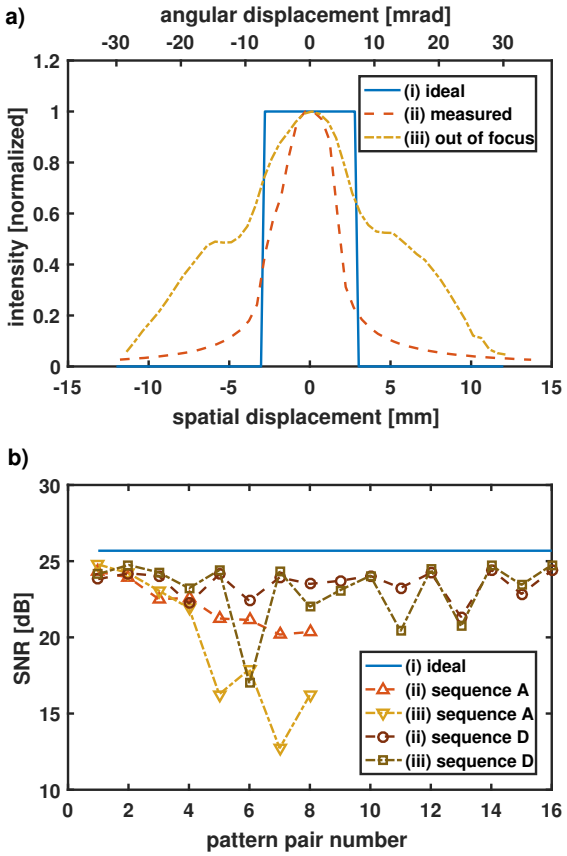


Fig. 9. Effect of interference: *a)* intensity profile of a single LED pixel at the receiver position, where (i) indicates the ideal profile, (ii) is the measured profile in the configuration used in section V-A, and (iii) is the profile of the same pixel when the projection was deliberately defocussed. *b)* Differential SNR for sequences A and D (compare Fig. 8a), for the different intensity profiles in *a)*.

on the transmitter. This effect may be even stronger if the optics create a blurred projection and the emissions from different pixels interfere upon propagation of the light through the room. A case of strong interference was created by moving the projection optics deliberately out of focus, resulting in profile (iii) in Fig. 9a).

Fig. 9b) shows the corresponding differential SNR. If the emission profile had a perfect top-hat shape without optical cross-talk or interference, then the differential SNR would be identical

for all pattern pairs and given by the dynamic range of the illumination versus the noise, which was 25.7 dB in this particular experiment and is indicated by the solid line. When comparing the experimentally measured differential SNR in the case of profile (ii) and (iii), we notice that sequence A is severely influenced. The last 4 pattern pairs (out of 8) of sequence A experience a drop in differential SNR by about 5 dB, and the average value for the sequence drops by 2.4 dB. In comparison, only 2 out of 16 pattern pairs in sequence D experience a strong SNR reduction, and the average drop of SNR of sequence D is only 0.4 dB. This shows that sequence D offers enhanced resilience against even severe interference between LED pixels.

### *C. Compatibility with lighting functionality*

Many VLC applications require dual use of the LEDs for communications and lighting. Therefore, flicker-free operation and dimming capability are mandatory. In the experimental section, patterns were displayed at 200 fps, which is already beyond visual flicker recognition, and all pattern sequences were flicker-free in our experiment due to the built-in Manchester encoding. Furthermore, operation at up to 30 kfps is possible with current technology [7]. If the frame rate is close to the threshold for visual flicker recognition ($\sim$60 fps), then there may be a difference in the flicker perceived from the different sequences, with sequence C likely to have the least and sequence D the most flicker. Dimming can be achieved through pulse width modulation (PWM) as shown in Fig. 10, *i.e.* each pattern is only displayed for a fraction of the frame time corresponding to the dimming level.

### *D. Compatibility with matrix-addressed arrays*

A traditional approach to electrically contact two-dimensional arrays of high brightness LEDs is matrix addressing, which currently provides better maturity and lower cost compared to active-matrix devices. In this case, the cathodes of the LEDs in each row of the array are interconnected via a metal track and the anodes of the LEDs in each column are also interconnected as shown

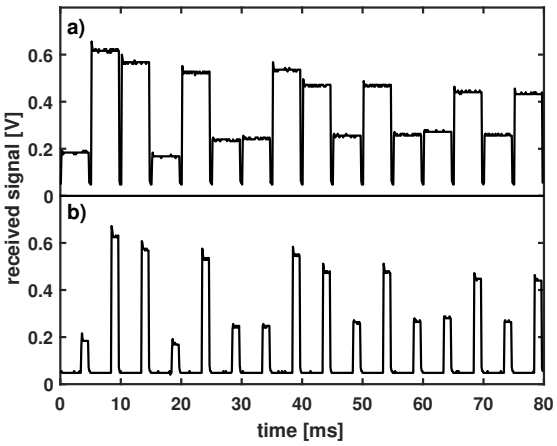


Fig. 10. Demonstration of dimming via PWM: pattern sequence A detected at row 11 and column 9 at *a)* full intensity and *b)* intensity dimmed to 25%.

in Fig. 11 [9]. An LED in the array will light up if its cathode is connected to ground (0 V) and its anode is connected to a positive voltage +V, see Fig. 11a. Complex patterns are traditionally displayed by line-scanning. However, for the purpose of positioning as described above, the individual patterns need to be displayed statically. Let $t_{k,l}$ be a pattern to be displayed by a matrix-addressed array, where $k$ denotes the rows and $l$ the columns of the array (note that the way we index $t$ here is different from sections II and III-A). Then any pattern that can be displayed statically by a matrix-addressed device has to fulfil equation (21):

$$t_{k,l} = 1,\ t_{k',l'} = 1 \quad \Rightarrow \quad t_{k,l'} = 1,\ t_{k',l} = 1 \tag{21}$$

Eq. (21) means that if two pixels are turned on that are not in the same row or column, then they force two other pixels to be turned on as well. One such pattern is illustrated schematically in Fig. 11b. We observe that all patterns of sequences A and D fulfil condition (21) and can therefore be displayed by matrix addressed devices. Pattern sequences B and C cannot be used with matrix-addressed arrays.

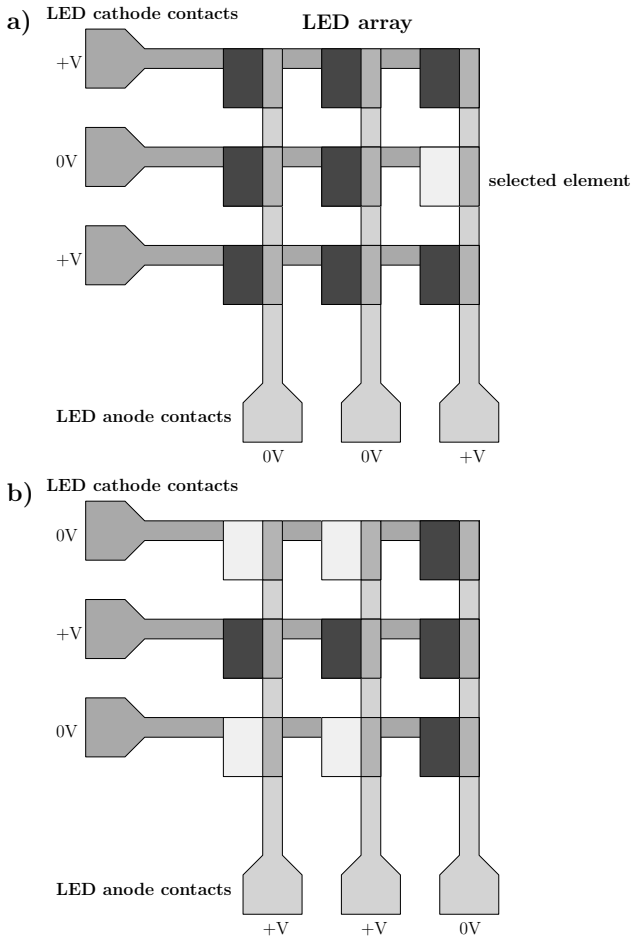


Fig. 11. Schematic illustration of a 3×3 matrix addressable LED array. *a)* a single LED is turned on and *b)* a pattern with four LEDs turned on.

## VI. INTERLEAVED DATA BROADCASTING

It has been shown previously that positioning with LED arrays can be used for space-domain multiple access to receivers with known locations [4], where the location information is fed back from the receiver to the transmitter. However, it may also be useful to broadcast information to any devices in the illuminated area even if their location is not known to the transmitter. Here it is described how such broadcasting can be interleaved with the positioning signal. Such an interleaved signal was used for the demonstration of a wirelessly controlled robot where all

TABLE II

FRAME STRUCTURE FOR INTERLEAVED POSITIONING AND BROADCASTING. INDIVIDUAL PATTERNS ARE REFERRED TO BY THE IDENTIFIERS USED IN FIGS. 2, 3, 4, AND 6.

| pattern number | before frame start | 1 | 2 | 3 | 4 | 5 | 6 | 7 | 8 | ... |
|---|---|---|---|---|---|---|---|---|---|---|
| frame for positioning | embedded clock | 1a | 1b | 1a | 1b | 2a | 2b | 3a | 3b | ... |
| | | positioning sequence | | | | | | | | |
| frame for broadcasting | embedded clock | 1a | 1b | 1b | 1a | $\begin{pmatrix} 1a & 1b \\ or & or \\ 1b & 1a \end{pmatrix}$ | | $\begin{pmatrix} 1a & 1b \\ or & or \\ 1b & 1a \end{pmatrix}$ | | ... |
| | | "1" | | "0" | | bit 1 | | bit 2 | | |

control functions were implemented through the LED illumination [17].

In principle, broadcasting can be achieved by applying exactly the same signal to all LEDs. However, it is desirable to keep equation (4). To enable this, data can be broadcasted with the patterns 1a and 1b of any of the above sequences. We can enable interleaved transmission and positioning by transmitting frames of length $n + 2$, where $n$ is the length of the positioning sequence. Then we can distinguish as follows:

- If the first four patterns of the current frame are (1a, 1b, 1a, 1b), then the patterns 3 to $n + 2$ in the frame are the positioning patterns
- If the first four patterns of the current frame are (1a, 1b, 1b, 1a), then the patterns 5 to $n + 2$ are Manchester encoded broadcast data, where a sequence of (1a, 1b) corresponds to "1" and a sequence (1b, 1a) corresponds to "0"

Between frames, an embedded clock signal can be sent for synchronisation. The frame structure is illustrated in table II for better clarity. Depending on the method for embedding the clock signal, the function of patterns number 1 and 2 in table II could be covered by the clock signal.

In our experimental demonstrations we used two patterns for clock synchronization, where the first pattern had all LEDs off and the second one had all LEDs on. This method is simple and reliable but violates equation (4) and requires the inclusion of patterns number 1 and 2 in the frame. It is possible to use a suitable sequence of patterns 1a and 1b as embedded clock which then requires a more sophisticated synchronization procedure.

## VII. Conclusion

Structured illumination with LED arrays enables wireless optical positioning and broadcasting with comparatively modest technological requirements. The receivers simply receive a Manchester-encoded bit sequence that contains the relevant information. The transmitters can be matrix-addressed or active-matrix LED arrays and position information or broadcast data is encoded using a simple set of illumination patterns. We developed pattern sequences for such positioning with sequence length $n = 2\log_2(N)$, $n = 3\log_2(N)$, and $n = 2\sqrt{N}$, where $N$ is the number of discrete spatial sites, each being addressed by one LED in our experimental implementation. While the shortest pattern sequences allow the fastest position update rate, it has been shown experimentally that by trading off the pattern sequence length an improvement of the SNR by about 2 dB is possible in typical conditions, and in situations of strong interference an improvement by 4 dB can be obtained. It was discussed how the same patterns can be used for interleaved data transfer to receivers in the illumination area. This scheme can provide the basis of a wireless optical infrastructure where mobile devices in a room are connected to and potentially controlled by the illumination.

## Appendix

In the case of a rectangular $n \times m$ array, we can give analyical expressions for the figures of merit for resilience against cross-talk, $\langle FOM \rangle$ and $\max(FOM)$, of pattern sequences A, B ($n \times n$ array), C (probabilistic average value), D and raster scanning. These expressions are

derived from Eqs. (16) and (17) as illustrated below.

$$\langle FOM\rangle_{\text{raster scan}} = \frac{1}{n^2m^2}\left(16nm - 12n - 12m + 8\right) \tag{22}$$

$$\max(FOM)_{\text{raster scan}} = \frac{16}{nm} \qquad n, m \geq 3 \tag{23}$$

$$\langle FOM\rangle_{\text{A}} = \frac{1}{2nm}\left(\frac{1}{\log_2(n)}\sum_{l=1}^{\log_2(n)}(2^l-1)(6n-4) + \frac{1}{\log_2(m)}\sum_{k=1}^{\log_2(m)}(2^k-1)(6m-4)\right) \tag{24}$$

$$\max(FOM)_{\text{A}} = \frac{n-1}{nm}(6n-4) \qquad \text{wlog } n \geq m \tag{25}$$

$$\langle FOM\rangle_{\text{B}} = \frac{1}{3n^2\log_2(n)}\left[\sum_{l=1}^{\log_2(n)}\left\{3(2^l-1)(6n-4) + 4(2^l-1)^2\right\} - 4\right] \tag{26}$$

$$\max(FOM)_{\text{B}} = \frac{n-1}{n^2}(6n-4) \tag{27}$$

$$\langle FOM\rangle_{\text{C}} = \frac{1}{nm}(4nm - 3n - 3m + 12) \tag{28}$$

$$\max(FOM)_{\text{C}} = \frac{1}{nm}(4nm - 3n - 3m + 12) \tag{29}$$

$$\langle FOM\rangle_{\text{D}} = \frac{1}{n^2m^2}(6nm^2 + 6n^2m - 20nm + 4n + 4m) \tag{30}$$

$$\max(FOM)_{\text{D}} = \frac{1}{nm}(12n - 8) \qquad \text{wlog } n \geq m \tag{31}$$

As an example, we illustrate the derivation of Eqs. (30) and (31). Look at Fig. 6 for reference. The first 4 patterns have one straight-line boundary between the regions with pixels on and pixels off. This boundary line has 4 edge pixels with each having 2 adjacent pixels with a different illumination state. Thus, following Eqs. (16) and (17), the contribution $FOM_{edge}$ of these four pixels is:

$$FOM_{edge} = \frac{4 \cdot 2}{nm} \tag{32}$$

The remaining pixels on this boundary have each 3 adjacent pixels with different illumination state. Along the first dimension, there are $2(n-2)$ of these pixels, and along the second dimension there are $2(m-2)$ of them. Thus, their contribution $FOM_{inner}$ to the overall $FOM$ is:

$$FOM_{inner} = \frac{2(n-2)\cdot 3}{nm} \qquad \text{dimension 1} \tag{33}$$

$$FOM_{inner} = \frac{2(m-2)\cdot 3}{nm} \qquad \text{dimension 2} \tag{34}$$

The overall $FOM$ of the first four patterns of sequence D is then:

$$FOM_{\mathrm{D},1^{st}} = FOM_{edge} + FOM_{inner} \tag{35}$$

All the other patterns of sequence D have two such straight boundary lines. Thus their $FOM$ is:

$$FOM_{\mathrm{D},2^{nd}} = 2FOM_{\mathrm{D},1^{st}} \tag{36}$$

And, therefore, $\max(FOM)_{\mathrm{D}} = FOM_{\mathrm{D},2^{nd}}$ which directly leads to Eq. (31). To derive Eq. (30), we need to count how many patterns of each type are contained in sequence D:

$$\begin{aligned}\langle FOM\rangle_{\mathrm{D}} = \frac{1}{n+m}\Bigg(&2FOM_{\mathrm{D},1^{st}}^{\text{dimension 1}} + 2FOM_{\mathrm{D},1^{st}}^{\text{dimension 2}} \\ &+ (n-2)FOM_{\mathrm{D},2^{nd}}^{\text{dimension 1}} + (m-2)FOM_{\mathrm{D},2^{nd}}^{\text{dimension 2}}\Bigg)\end{aligned} \tag{37}$$

This leads directly to Eq. (30). All of the other equations (22)–(31) are derived by similar arguments as outlined here on the example of sequence D.

Below are the proofs of equations (8), (6) and (7). Similar to equation (12), consider bitstreams arranged in a matrix $t$:

$$t = \begin{bmatrix} t_{1,1} & t_{1,2} & \dots & t_{1,n} \\ t_{2,1} & t_{2,2} & \dots & t_{2,n} \\ \vdots & & & \\ t_{2^m,1} & t_{2^m,2} & \dots & t_{2^m,n} \end{bmatrix} \tag{38}$$

Please observe:

1) Any permutation of rows or columns in $t$ does not change the validity of equations (2), (3) and (4)
2) If all bits are inverted, then equations (2), (3) and (4) are still fulfilled
3) And therefore, wlog $T_{pat} \leq 2^{m-1}$ in equation (4)

Therefore, we can reorder $t$ to the following form:

$$t = \begin{bmatrix} & 0 \\ A & \vdots \\ & 0 \\ B & C \end{bmatrix} \tag{39}$$

where A and B are $(2^m) \times (n-1)$ matrices and C is a vector of length $2^m$ and $\sum C = T_{pat}$. Equation (3) implies:

$$\begin{aligned} \sum A &= \sum B + T_{pat} \\ \Rightarrow T_{pat} &= \sum A - \sum B \\ &= \sum A + \sum B - 2\sum B \\ &= (n-1)T_{pat} - 2\sum B \\ \Rightarrow \sum A &= \frac{n-1}{2} T_{pat} \end{aligned}$$

For the second last step, we used equation (4). Note that equation (3) implies that $\sum A = 2^m T_{seq}$ and from this follows equation (6):

$$T_{seq} = \frac{n}{2^m} T_{pat} \tag{6}$$

The left hand side of the equation is an integer. For uneven $n$, the right hand side of the equation can only be an integer if $T_{pat} \geq 2^m$. However, this is in contradiction to $T_{pat} \leq 2^{m-1}$ which is necessary to write $t$ in the form (39). Hence $n$ needs to be even and equation (7) is thus shown.

Any pattern sequence that fulfils equations (2) and (3) automatically fulfils:

$$\binom{n}{T_{seq}} \geq 2^m \tag{40}$$

This is also true for $n = n_{min}$. We can maximise the left hand side by choosing $T_{seq} = \lfloor n_{min}/2 \rfloor$ which leads directly to equation (8).

## REFERENCES


[1] "Data available online, DOI=http://dx.doi.org/10.15129/8231a87a-8714-4560-b22d-ee7584726868," 2017.

[2] T.-H. Do and M. Yoo, "An in-depth survey of visible light communication based positioning systems," *Sensors*, vol. 16, no. 5, p. 678, 2016. [Online]. Available: http://www.mdpi.com/1424-8220/16/5/678

[3] J. Armstrong, Y. A. Sekercioglu, and A. Neild, "Visible light positioning: a roadmap for international standardization," *IEEE Communications Magazine*, vol. 51, no. 12, pp. 68–73, December 2013.

[4] J. Herrnsdorf, M. J. Strain, E. Gu, R. K. Henderson, and M. D. Dawson, "Positioning and space-division multiple access enabled by structured illumination with light-emitting diodes," *Journal of Lightwave Technology*, vol. 35, no. 12, pp. 2339–2345, June 2017.

[5] M. T. Taylor and S. Hranilovic, "Angular diversity approach to indoor positioning using visible light," in *2013 IEEE Globecom Workshops (GC Wkshps)*, Dec 2013, pp. 1093–1098.

[6] J. K. Park, T. G. Woo, M. Kim, and J. T. Kim, "Hadamard matrix design for a low-cost indoor positioning system in visible light communication," *IEEE Photonics Journal*, vol. 9, no. 2, pp. 1–10, April 2017.

[7] J. Herrnsdorf, J. J. D. McKendry, E. Xie, M. J. Strain, I. M. Watson, E. Gu, and M. D. Dawson, "High speed spatial encoding enabled by cmos-controlled micro-led arrays," in *2016 IEEE Photonics Society Summer Topical Meeting Series (SUM)*, July 2016, pp. 173–174.

[8] J. Herrnsdorf, M. J. Strain, E. Gu, and M. D. Dawson, "Concept of a gan-led-based positioning system using structured illumination," in *2015 IEEE Photonics Conference (IPC)*, Oct 2015, pp. 28–29.

[9] Z. Gong, H. X. Zhang, E. Gu, C. Griffin, M. D. Dawson, V. Poher, G. Kennedy, P. M. W. French, and M. A. A. Neil, "Matrix-Addressable Micropixellated InGaN Light-Emitting Diodes With Uniform Emission and Increased Light Output," *IEEE Trans. Electron. Dev.*, vol. 54, no. 10, pp. 2650–2658, 2007.

[10] H. W. Choi, C. W. Jeon, and M. D. Dawson, "High-Resolution 128×96 Nitride Microdisplay," *IEEE Electron. Dev. Lett.*, vol. 25, no. 5, pp. 277–279, 2004.

[11] Q. Wang, D. Giustiniano, and D. Puccinelli, "An open source research platform for embedded visible light networking," *IEEE Wireless Communications*, vol. 22, no. 2, pp. 94–100, April 2015.

[12] S. Li, A. Pandharipande, and F. M. J. Willems, "Two-way visible light communication and illumination with leds," *IEEE Transactions on Communications*, vol. 65, no. 2, pp. 740–750, Feb 2017.

[13] J. Herrnsdorf, J. J. D. McKendry, S. Zhang, E. Xie, R. Ferreira, D. Massoubre, A. M. Zuhdi, R. K. Henderson, I. Underwood, S. Watson, A. E. Kelly, E. Gu, and M. D. Dawson, "Active-Matrix GaN Micro Light-Emitting Diode Display with Unprecedented Brightness," *IEEE Trans. Electron Dev.*, vol. 62, no. 6, pp. 1918–1925, 2015.

[14] M.-J. Sun, M. P. Edgar, D. B. Phillips, G. M. Gibson, and M. J. Padgett, "Improving the signal-to-noise ratio of single-pixel imaging using digital microscanning," *Opt. Express*, vol. 24, no. 10, pp. 10 476–10 485, May 2016. [Online]. Available: http://www.opticsexpress.org/abstract.cfm?URI=oe-24-10-10476

[15] Z. Zhang, X. Wang, G. Zheng, and J. Zhong, "Hadamard single-pixel imaging versus fourier single-pixel imaging," *Opt. Express*, vol. 25, no. 16, pp. 19 619–19 639, Aug 2017. [Online]. Available: http://www.opticsexpress.org/abstract.cfm?URI=oe-25-16-19619

[16] S. Zhang, S. Watson, J. J. D. McKendry, D. Massoubre, A. Cogman, E. Gu, R. K. Henderson, A. E. Kelly, and M. D. Dawson, "1.5 gbit/s multi-channel visible light communications using cmos-controlled gan-based leds," *Journal of Lightwave Technology*, vol. 31, no. 8, pp. 1211–1216, April 2013.

[17] J. Herrnsdorf, M. J. Strain, and M. D. Dawson, "Control of automated systems with a structured light illumination source," in *2016 IEEE Photonics Conference (IPC)*, Oct 2016, pp. 560–561.

**Johannes Herrnsdorf** (M'16) received the Dipl. Phys. degree from ETH Zürich in 2008 and the PhD degree in physics from the University of Strathclyde, Glasgow, in 2012. He is working on GaN micro-LEDs for communications and advanced imaging technology.

**Martin Dawson** (M'85-SM'98-F'09) received the PhD degree in physics from Imperial College, London, in 1985. He has worked at North Texas State University, Denton, the University of Iowa, Iowa City, SLE Oxford and the University of Strathclyde, where he has been a professor since 2001. He is director of research at the University of Strathclyde Institute of Photonics and Head of the Fraunhofer Center for Applied Photonics.

**Michael Strain** is a senior lecturer in photonic semiconductor devices at the University of Strathclyde. He received a MASc and PhD in photonics from the University of Toronto and the University of Glasgow respectively. His research interests include: micro-LED arrays for high speed structured illumination, micro and nano-fabrication techniques for integrated optical devices across the III-V and silicon material platforms, hybrid device integration and on-chip semiconductor lasers.